Supporting Information

Overall Structure Construction of Intervertebral Disc Based on Highly Anisotropic Wood-Hydrogel Composite Materials with Mechanical Matching and Buckling Buffering

*Jinming Liu,[a] Dingqian Wang,[a] Yanyan Li,[a] Ziqi Zhou,[a] Dongyue Zhang,[a b] Jianshu Li,[a b] * and Hetao Chu[a] **

[a] College of Polymer Science and Engineering, Sichuan University, Chengdu 610065, China

[b] State Key Laboratory of Polymer Materials Engineering, Sichuan University, Chengdu 610065, China

*To whom correspondences should be addressed. Email: jianshu_li@scu.edu.cn

(J. S. Li), chuht@scu.edu.cn; chuhetao@outlook.com (H. T. Chu).

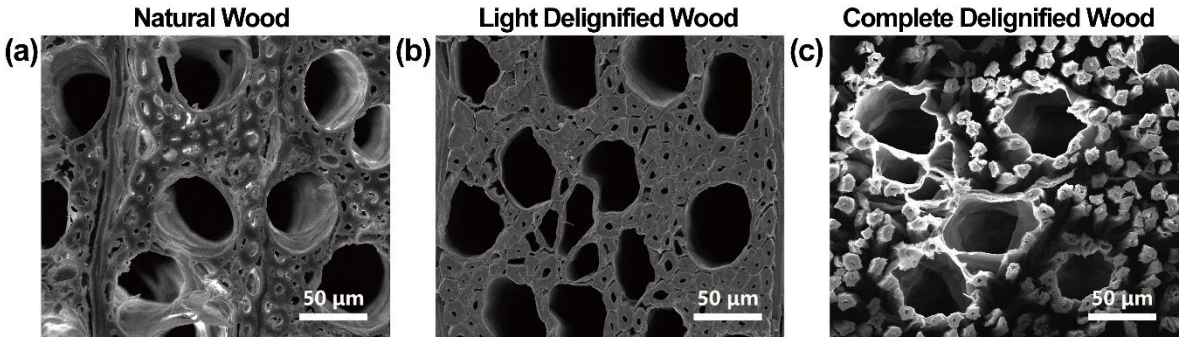

Figure S1. SEM images of (a) natural beech wood, (b) lightly delignified wood, and (c) fully delignified wood. The SEM images illustrate the unique microstructure of natural beech wood with different treatments.

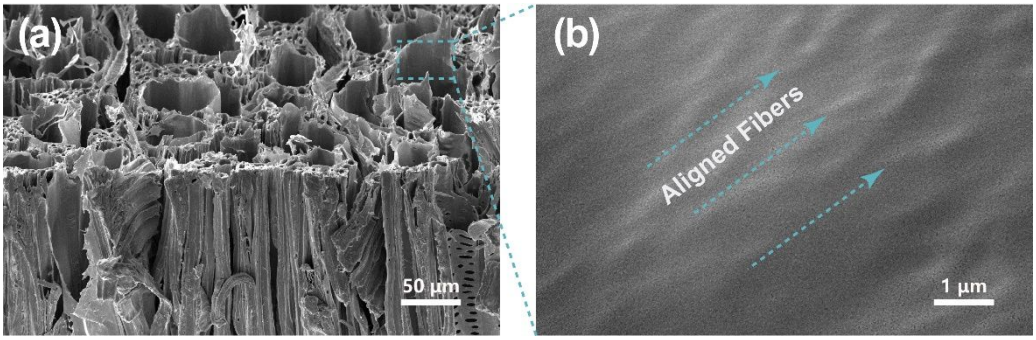

Figure S2. Morphology of cellulose framework. The SEM images of (a) stereoscopic structure and (b) local microstructure of the square, which shows that the cellulose framework maintains the stable 3D structure and aligned nanocellulose fibers are arranged in order.

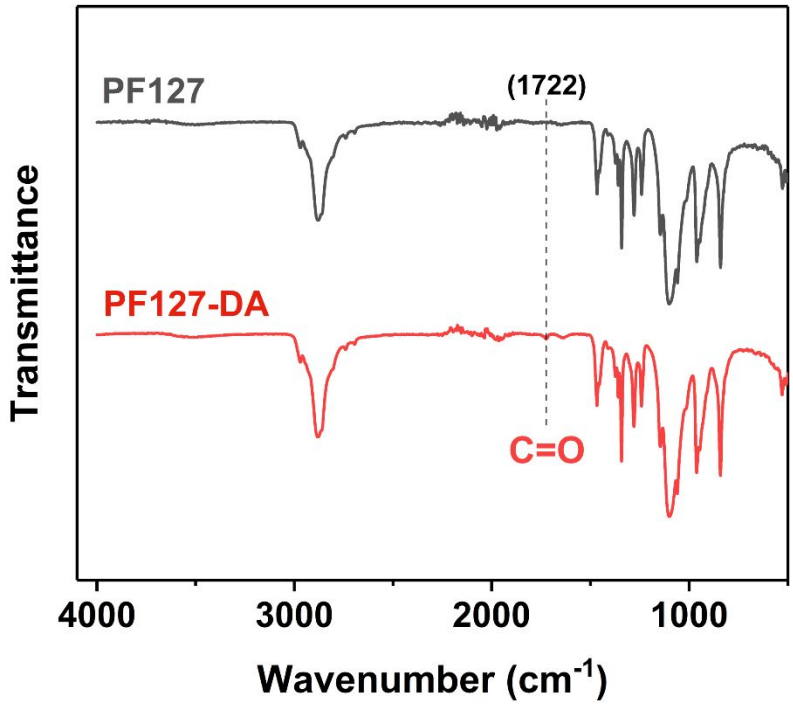

Figure S3. FTIR pattern of PF127 and PF127-DA. Compared with the original FTIR spectrum of PF127, there emerge a new characteristic C=O absorption peak at 1722 cm^{-1} from the acryloylation reaction.

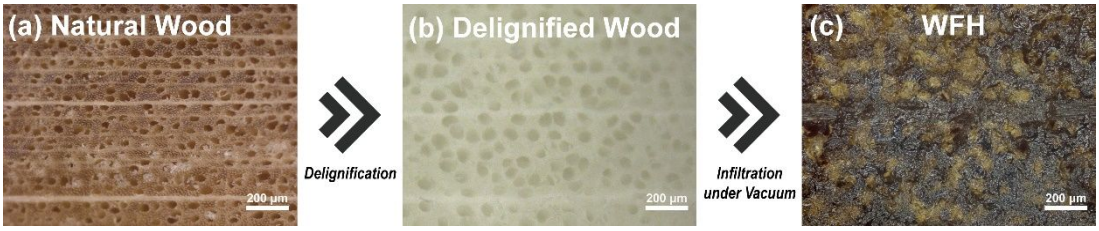

Figure S4. Optical images of different wood during this process. The surface morphologies of (a) natural beech wood, (b) completely delignified wood, and (c) WFH. During this treatment process, the pores of natural wood are opened and filled.

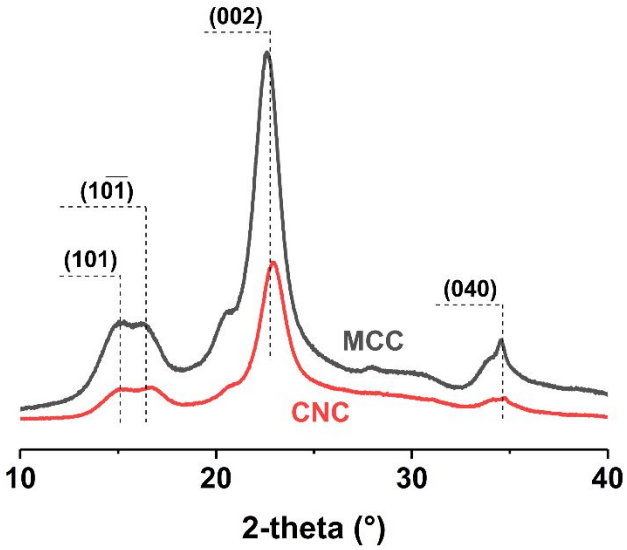

Figure S5. XRD pattern of MCC and CNC. The crystal of CNC is consistent with that of MCC, which illustrates that the chemical treatment did not destroy the crystal structure.

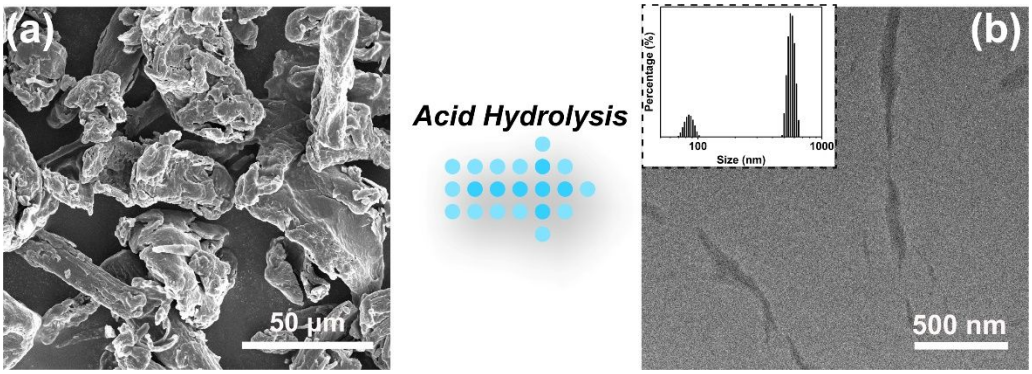

Figure S6. Morphologies of MCC and CNC. (a) The SEM images of MCC whose sizes are about tens of microns. (b) The TEM images and DLS analysis (inset) of CNC, which both reveal the typical rod-like structures with diameters of about 80 nm and length of about 500 nm.

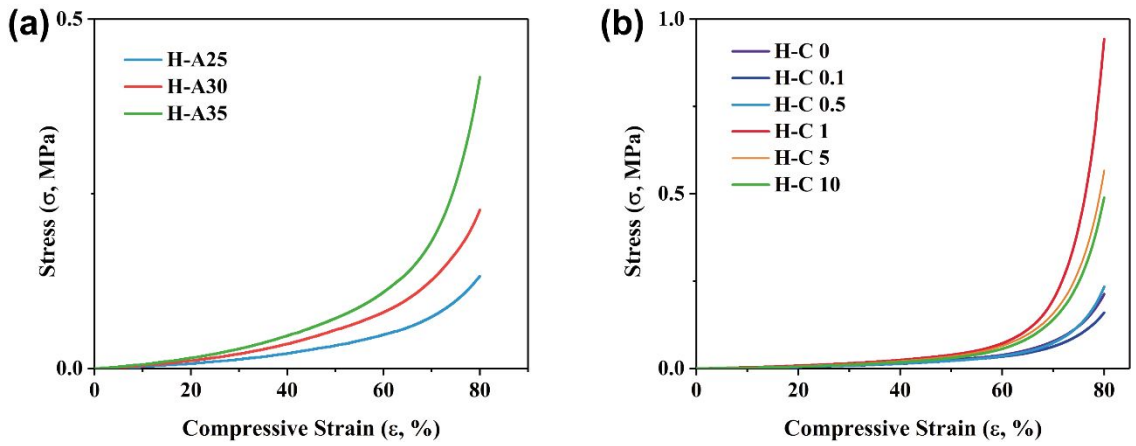

Figure S7. Mechanical curves of PAM hydrogels with varied content of (a) AM monomer and (b) CNC. Considering the balance between component content and mechanical properties, 30 wt% AM content and 1 wt% CNC were selected in this study.

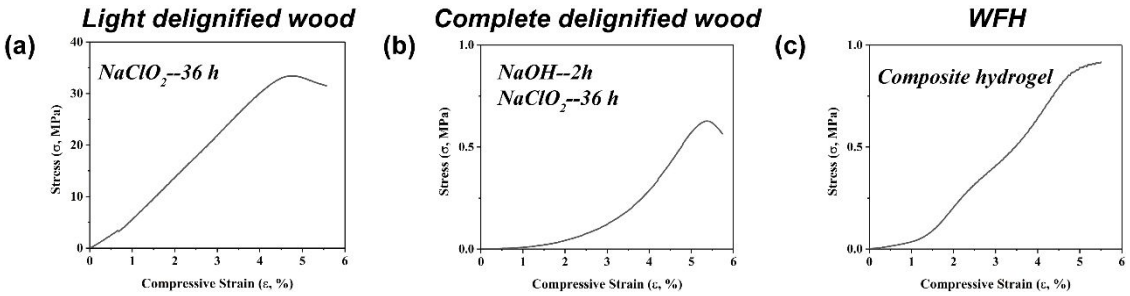

Figure S8. Mechanical properties of different wood-based materials. The compressive curves of (a) light delignified wood, (b) complete delignified wood, and (c) WFH. The materials are softened with the degree of delignification deepening, and mechanical performances slightly improve after compound treatment.

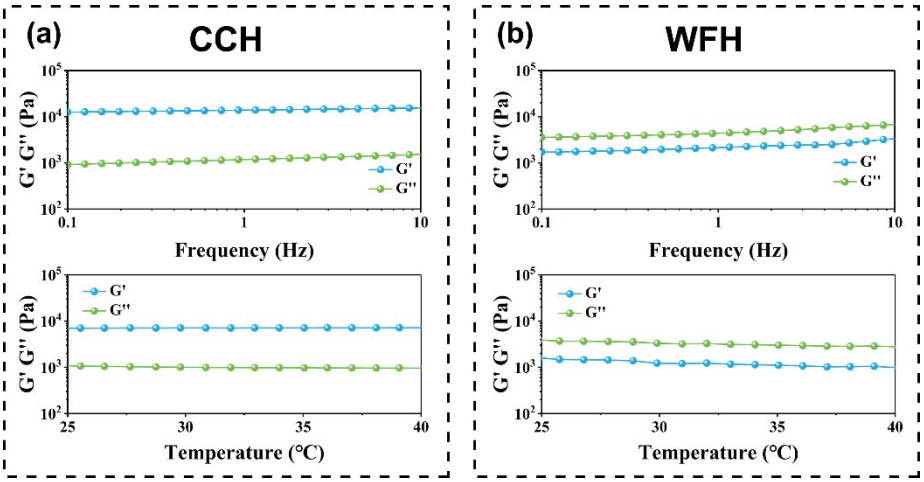

Figure S9. G’ and G’’ of CCH and WFH tested under various conditions. (a) CCH and (b) WFH both exhibit a stable condition in the range of 1-10 Hz and 25-40 °C.

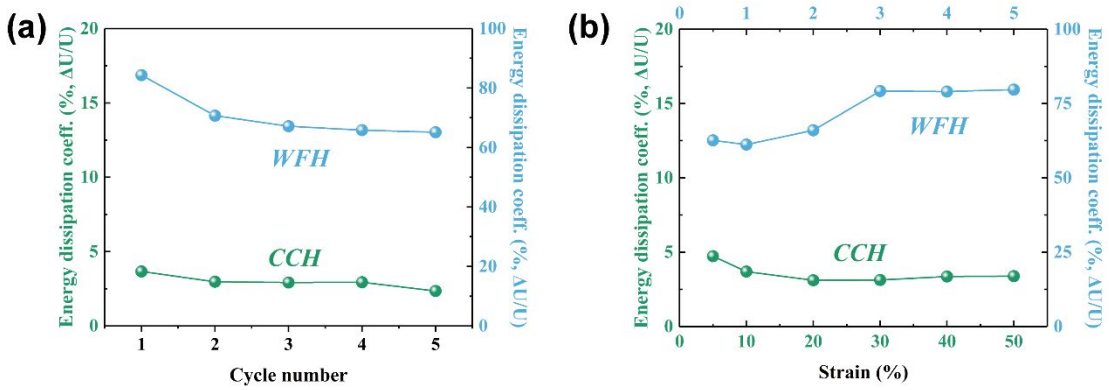

Figure S10. Energy dissipation coefficients calculated by the mechanical hysteresis of (a) cyclic loading-unloading test and (b) progressive loading-unloading test.

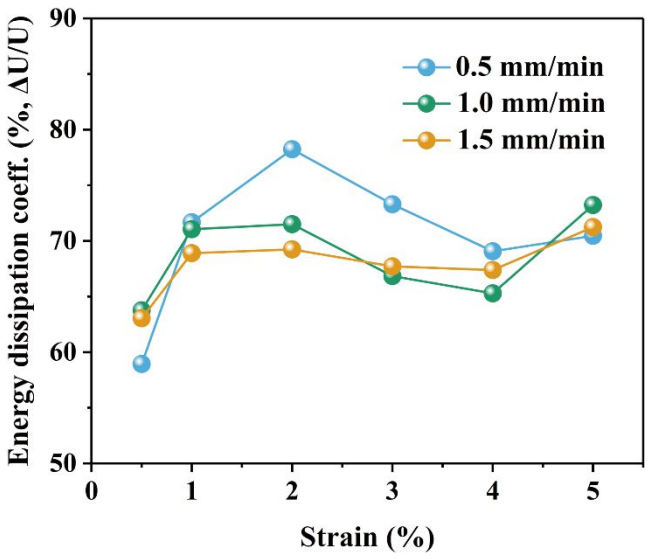

Figure S11. Energy dissipation coefficients calculated by the mechanical hysteresis of progressive loading-unloading test at varying compressive velocities.

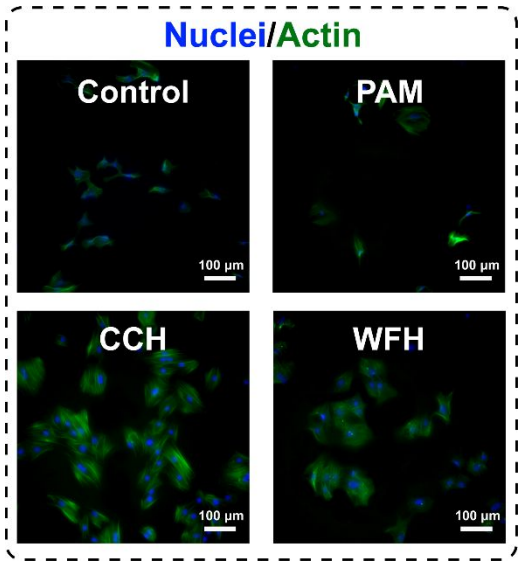

Figure S12. Cell morphology cocultured with varied groups conducted by fluorescent staining on Day 2. (Blue nuclei: Hoechst 33342; Green actin: FITC phalloidin)

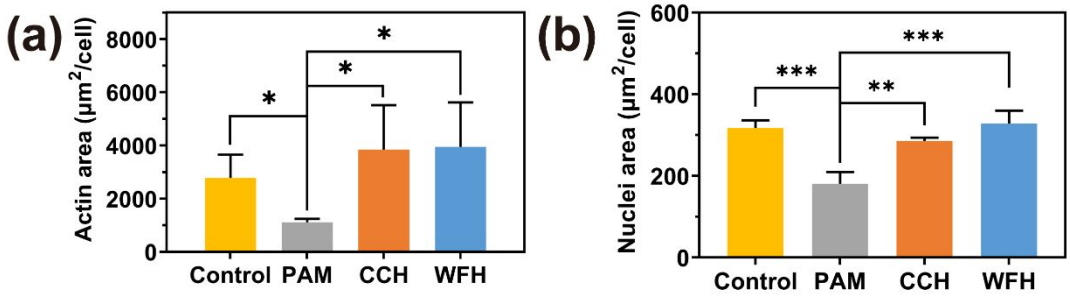

Figure S13. The (a) nuclei and (b) actin areas are calculated using responding fluorescent chromatogram on Day 4. Error bars represent as mean ± SD, n = 3. *p < 0.05, **p < 0.01, ***p < 0.001.